Ceramic Bonding Interface under Shear–Compression Stress: Ultra-High-Speed Imaging Contribution

Hugo Lambert, Stéphane Corn, Romain Léger, Patrick Ienny, Pierre Slangen, Michel Fages

Ceramic bonding interface under shear-compression stress: UHSI contribution

H.Lambert [1,2], S.Corn [3], R.Léger [3], P.Ienny [3], P.Slangen [4], M.Fages [1,2]

[1] Laboratory Bioengineering and Nanosciences, University of Montpellier, Montpellier, France

[2] Department of Prosthetic Dentistry, Facultu of Odontology, Montpellier University, France

[3] LMGC, Univ Montpellier, IMT Mines Ales, Ales, France

[4] EuroMov Digital Health in Motion, Univ Montpellier, IMT Mines Ales, Ales, France

Corresponding Author: H.Lambert, Department of Prosthodontics, Faculty of Odontology, Montpellier University, 545 av. du Professeur J.L.Viala, 34193 Montpellier Cedex 5 France. Email : dr.hugo.lambert@hotmail.com

This article has been first published online on December 23rd, 2022 in Journal of Dental Research (SAGE). https://doi.org/10.1177/00220345221138500

Abstract:

The aim of this study is to visualize and characterize by ultra-high-speed imaging (UHSI) the failure phenomena at the resin–ceramic bonding interface of lithium disilicate (LiSi2) samples bonded with gold-standard protocol (Monobond Plus [MB]) and the nontoxic one (Monobond Etch & Prime [MEP]) subjected to mechanical loading. Unprecedented frame rate, image resolution, and recording time were reached by using the most advanced UHSI camera. The finite element analysis (FEA) of the proposed mechanical test confirmed that the specific design of our samples enables a combined shear and compression stress state, prone to test the bonding interface while being close to physiological stresses. Ten LiSi2 samples were pretreated by gold standard (MB, n = 5) and self-etching primer (MEP, n = 5). Axial compression loading gradually increased until catastrophic failure was performed. As shown by the FEA, the angle between the bonding interface and load direction leads to shear–compression stresses at the resin–ceramic bonding interface. Failure was recorded by UHSI at 300,000 fps. All recorded images were analyzed to segregate events and isolate the origin of fracture. For the first time, thanks to the image recording setup, it was observed that debonding is the first event before breakage, highlighting that sample fracture occurs by interfacial rupture followed by slippage and cohesive failure of materials. Failure mode could be described as mixed. MEP and MB showed similar results and behavior.

Keywords: imaging, biomaterials, adhesives, silanes, biomechanics, Finite Element Analysis (FEA)

1 Introduction:

Ceramic adhesive restorations (CARs) are widely used for aesthetic treatment. Their good optical properties, translucency, biocompatibility, and high mechanical properties have expanded the range of their indications

(Guimarães et al. 2018). CARs are indicated for veneers as well as endodontically treated teeth, notably on severely damaged posterior teeth (Fages and Bennasar 2013; Decerle et al. 2014; Fages, Raynal, et al. 2017). The success of CARs on posterior teeth has already been demonstrated (Magne et al. 1999; Fages, Raynal, et al. 2017). Nevertheless, the bonding interface, involving ceramic and resin cement, seems to be the main trigger causing the majority of encountered failures (Magne and Douglas 1999; Breschi et al. 2008; Yu and Wang 2008; Lafuente 2012; Fages, Corn, et al. 2017; Yao et al. 2019). The literature is rich about ceramic fracture and ceramic debonding under mechanical stress (Burke 1999; Pineda-Vásquez et al. 2019; Venturini et al. 2019). In most of these studies, crack initiation is not detected with sufficient accuracy. Shear–compression test appears to be close to the clinical situation where shear may occur at interfaces angled from the loading direction. Detecting the cause of crack initiation may help to better understand the failure phenomena of CARs.

Ultra-high-speed imaging (UHSI) appears as the best solution to segregate events and isolate the first one happening. Resin–dentin interface failure under different mechanical stresses had been observed with UHSI but without providing those answers (Sidhu et al. 1999; Griffiths et al. 2000).

The latest improvements of UHSI for both higher frame rate (320,000 fps) and image quality (resolution and dynamic range) will allow isolating and characterizing the first event and those following until catastrophic failure.

For the second interrogation, shear and tensile bond strength tests (macro- or micro-test; SBS, TBS, μSBS, μTBS) are usually static tests. They generate a more or less homogeneously distributed stress field that could deliver an indicative interfacial adhesion load. According to Guggenbül et al. (2021), “μSBT could be more suitable for testing the adhesion of resin-based materials to ceramics.” Shear stresses are believed to be major stresses involved in in vivo bonding failures in CARs (Guggenbühl et al. 2021). In this sense, we demonstrated by a preliminary finite element analysis presented in this study the interest of our original lithium disilicate (LiSi2)

bonded sample and the benefit of a 45° resin bonding interface. The resulting shear–compression stress field induced to the resin bonding interface is closer to clinical reality than other interfacial mechanical tests (TBS, μTBS, SBS, μSBS tests) (Burke 1999; Blatz et al. 2003; Chi et al. 2017; Pineda-Vásquez et al. 2019; Venturini et al. 2019; Guggenbühl et al. 2021).

Concomitantly, with clinical consideration, we decided to compare 2 ceramic pretreatments. Classically, the ceramic intaglio is conditioned with hydrofluoric acid (HF), allowing a selective elimination of the vitreous matrix causing a roughness of the ceramic and more surface energy (Siqueira et al. 2019). Then, a primer containing organo-silane is applied to promote bifunctional and durable adhesion (Blatz et al. 2003; Dejak and Mlotkowski 2008; Lise et al. 2015). However, HF is toxic for the human body and the environment, and its use has been prohibited in several countries (Özcan et al. 2012; Kalavacharla et al. 2015; Maier et al. 2019; Dapieve et al. 2020). A recent nontoxic self-etching glass-ceramic primer, Monobond Etch & Prime (MEP; Ivoclar-Vivadent), was proposed to secure and simplify the bonding protocol. Ammonium polyfluoride contained in MEP is milder than HF and generates a less rough surface (El-Damanhoury and Gaintantzopoulou 2018). However, this single-component product allows etching and silanizing in 1 step, with the same application time regardless of the glass ceramic (Maier et al. 2019).

The purpose of the present study was to visualize and characterize by UHSI the failure phenomena at the resin bonding interface by shear–compression test of LiSi2 samples bonded with gold-standard protocol and the new nontoxic alternative.

2 Material and method

2.1 Samples

Ten discs (diameter 18.5 mm, thickness 4 mm) of LiSi2 (IPS E.max press; Ivoclar-Vivadent) were diametrically cut in half with a laboratory saw (Isomet 2000; Buehler). Samples were divided in 2 groups. Intaglio pretreatment and bonding protocol were achieved according to the manufacturer recommendations. For the first group (n = 5), surfaces were etched for 20 s using 5% HF (IPS Ceramic Etching Gel; Ivoclar-Vivadent), rinsed off, and thoroughly dried. Then a thin coat of silane agent (Monobond Plus [MB]; Ivoclar-Vivadent) was applied using a microbrush. The silane was allowed to react for 60 s, and then a strong stream of air was used to disperse any remaining excess. The second group (n = 5) received the MEP (Ivoclar-Vivadent) 1-step ceramic primer. The MEP was applied on the adhesive surface using a microbrush and agitated into the surface for 20 s. It was left to react for another 40 s. Then the MEP was thoroughly rinsed off with water and the restoration was dried with a strong jet of water- and oil-free air for 10 s. Bonding protocol was the same for each sample, regardless of the conditioning treatment. Samples parts were bonded (Variolink Esthetic DC Neutral; Ivoclar Vivadent), and resin was light cured 1 min with a 1,200-W light-polymerizing unit (Bluephase Style 20i; Ivoclar-Vivadent) on each face. Ceramic resin bonding interface thickness was measured as 600 µm. Then, bonded discs were cut to obtain 2 parallel surfaces at the top and bottom of each sample and a 45° inclined bonding resin interface according to the finite element analysis (FEA) presented hereafter (Fig. 1).

2.2 Mechanical test

As illustrated in Figure 1, samples were submitted to a compression loading performed at a crosshead speed of 1 mm/min on a Zwick ZH010 testing machine (ZwickRoell GmbH) equipped with a 10-kN load cell. This test allows the bonded layer to be submitted to a shear–compression stress state. A 20-N preload was applied to the sample before the test. During the test, force and displacement were continuously recorded up to failure. The stiffness of samples in kN/mm is also evaluated between 0.3 and 0.5 mm of displacement.

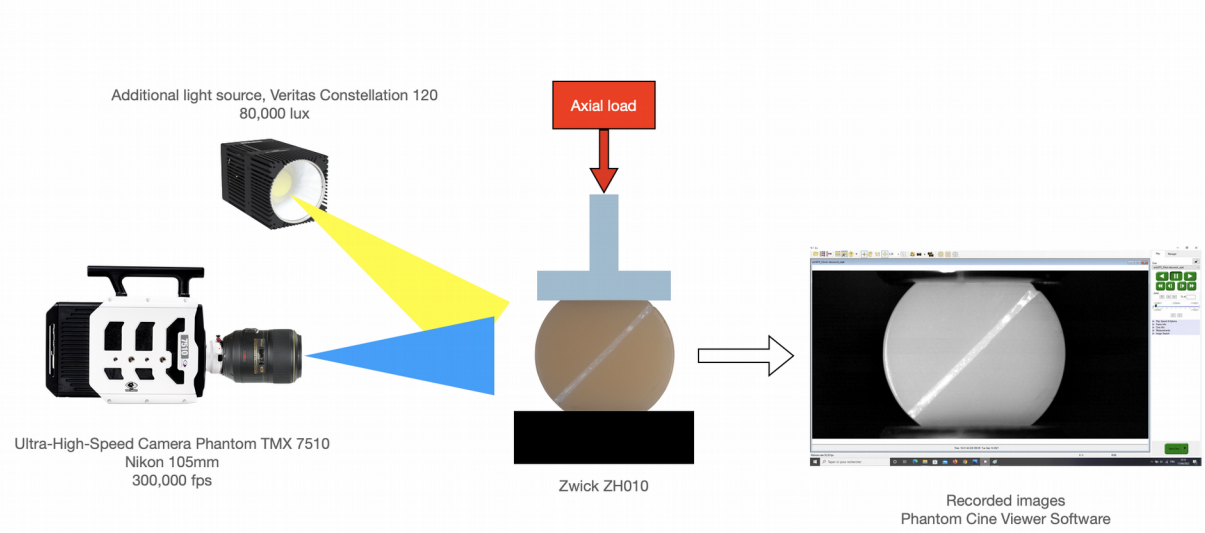

Figure 1. Scheme of the mechanical and optical setup.

2.3 Ultra-High-Speed Imaging

The fracture phenomena were recorded with a UHS Phantom TMX7510 camera (Phantom TMX7510; Vision Research). This camera has 76 Gpix/s throughput, offering 1,280 × 800 back-side illuminated (BSI; 18.5 µm) CMOS pixels at 76 kfps, which was equipped with a 105-mm magnification macro lens (Nikon) and using image resolution of 640 by 320 pixels, a frame interval of 3.33 µs, at a maximum rate of 300,000 fps at this resolution mode thanks to 2 × 2-pixel binning. This mode ensures sensitivity and leads to shorter exposure time. Binning also reduces resolution in order to deal with ultra-high-speed imaging frame rates. The BSI CMOS of the TMX 7510 with 512-GB onboard memory can then tackle frame rates and resolution of in situ image storage (ISIS) cameras but with huge image storage in a rolling memory buffer. Additional light source (Veritas Constellation 120; IDT Europe) delivered 80,000 lux of cold light at 1 m to obtain the best-recorded image by allowing a 2-µs exposure time to freeze the object displacement (Fig. 1). During the test, the camera was continuously recording images in onboard 512-GB memory. When memory gets “full,” recording continues by cycling back to the beginning, constantly overwriting itself (FIFO rolling buffer mode until the camera is triggered). For these tests, the trigger stopped the record and enabled saving all required frames present in the rolling memory buffer before and after the trigger event (e.g., a sudden decrease of the force at break or a crack sound). All the captured images were examined thanks to the dedicated software (Phantom Camera Control [PCC]; Vision Research) to chronologically identify different events until catastrophic failure.

2.4 Finite Element Analysis (FEA)

A numerical model was developed using Comsol Multiphysics Finite Element software, in order to calculate and analyze the stress state inside a sample subjected to the proposed mechanical test, with a particular interest at the resin–ceramic bonding interface. The modeled geometry corresponds to a ceramic disk (diameter 18.5 mm,

thickness 4 mm) diametrically split in 2 halves separated by a 600-µm resin joint and cropped to a 15-mm total height. The mechanical behaviors of both ceramic and resin were assumed linear and elastic before failure. Displacement continuity at the interfaces was considered in the model, which corresponds to perfectly adhesive interfaces. According to average values of the literature, the Young's modulus of the ceramic (respectively, the resin) was set to 80 GPa (respectively, 8 GPa) and the Poisson's ratio to 0.2 (respectively, 0.3). As illustrated in Figure 2A, upper and bottom flat surfaces are subjected to a 10-kN evenly distributed axial compression load (bottom surface being fixed for stability). The joint angle (α) was defined as a variable design parameter in the finite element (FE) model in order to assess its influence on the stress state inside the sample. According to the plane stress hypothesis, a 2-dimensional FE mesh has been produced. A mesh convergence study has been carried out, leading to 7,914 elements (6,314 triangles, 1,600 quadrangles), with a denser mesh near the resin–ceramic interfaces, as displayed in Figure 2B (for α = 45°). The FE parametric resolutions confirmed that the gradual variation of the joint angle from 0 to 45 degrees enables increasing the amount of shear stress inside the resin (from zero up to a value higher than compression stress), as plotted in Figure 2A. Thus, because higher shear stresses are prone to trial the bonding interface (for a given axial load value), the joint angle was subsequently set at 45° for the samples designed in that study. A FE plot of the shear strain distribution in the sample for α = 45° (Fig. 2C) corroborates that the shear strain is discontinuous at the bonding interface and is higher in the resin than in the ceramic.

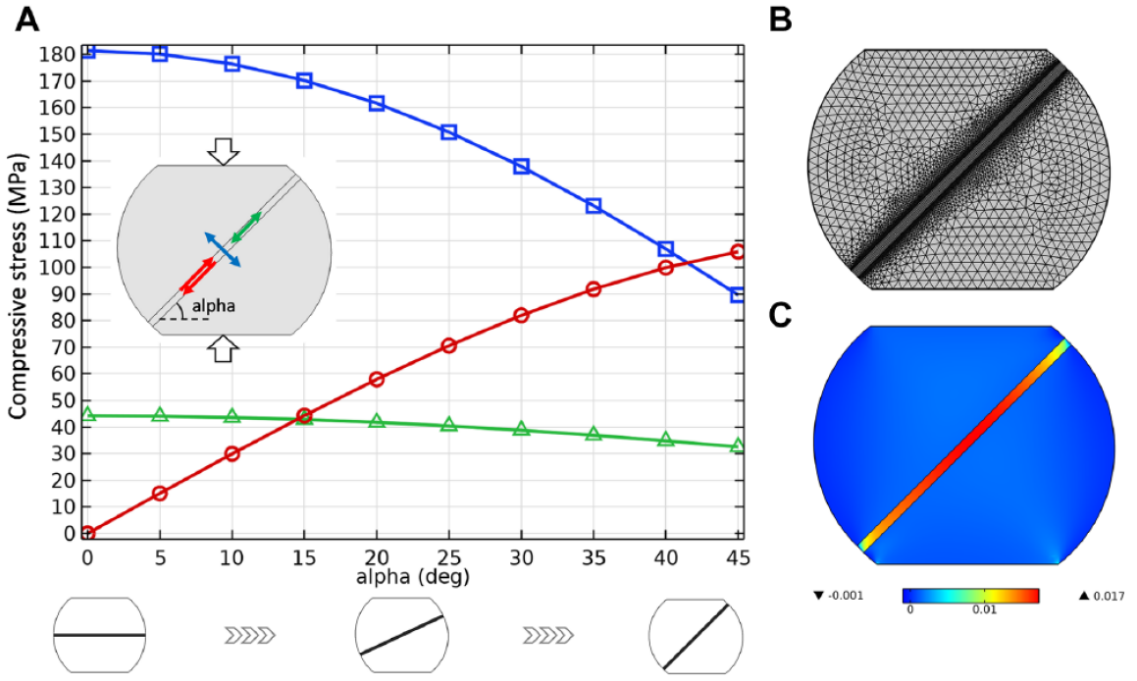

Figure 2. FE Analysis (A) Compressive stress (in MPa) at resin central point versus joint angle (α, in degrees) for a 10-kN compression load. Green triangles (respectively, blue squares) correspond to direction along (respectively, across) the joint. Red circles correspond to the shear component of stress. (B) Finite element (FE) mesh (displayed for α = 45°). (C) FE plot of the shear strain in the sample (displayed for α = 45°), highlighting the highest shear strain inside the resin.

3 Results

3.1 Mechanical tests

Load/displacement curves for the 2 groups of samples are shown in Figure 3. Fracture and stiffness results are available in the Appendix. Stiffness is obtained by a linear regression performed on the initial slope (<0.2 mm) of each curve while strength is the maximum force. The shape of curves is similar for both MEP and MB samples, while load at break differs much more. The average strength for MB (respectively, MEP) is 7,850 N (respectively, 8,690 N) with a standard deviation of 1,420 N (respectively, 860 N). The average stiffness for MB (respectively, MEP) is 16.1 kN.mm -1 (respectively, 15.9 kN.mm -1) with a standard deviation of 0.3 kN.mm -1 (respectively, 0.4 kN.mm -1).

For all tested samples, visual observations revealed an adhesive failure where 1 face is covered by bonding resin while the opposite side is raw ceramic.

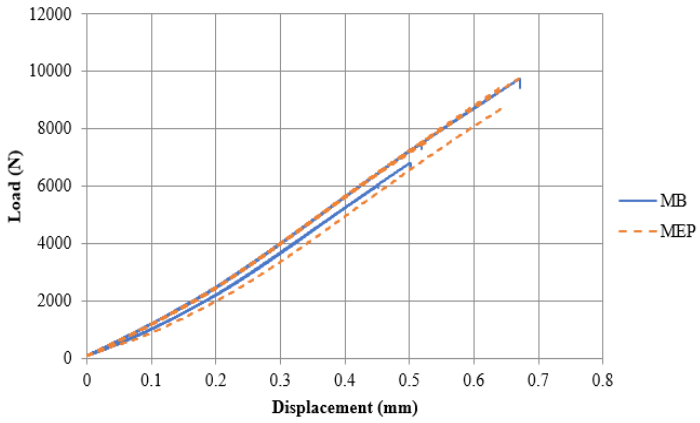

Figure 3. Load/displacement curves of each Monobond Plus (MB) and Monobond Etch & Prime (MEP) sample submitted to compression/shear test.

3.2 UHSI

Debonding, fracture initiation, and propagation were observed thanks to extreme frame rate and sensitivity of the UHSI camera. All results are presented in Figures 4 and 5 and multimedia components. The first picture of the illustration is the one before the first event observable in the sample. Each picture following corresponds to the frame interval 3.33 µs later, and various foci were done to highlight phenomena.

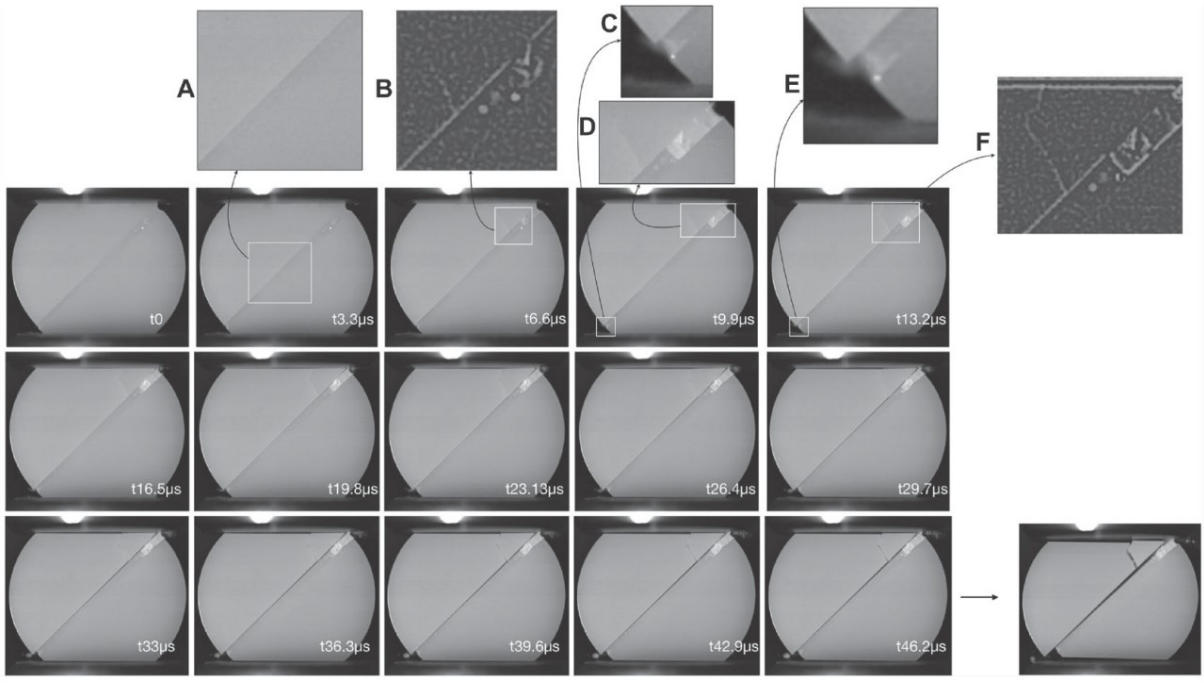

Figure 4. Sequence of successive images recorded by ultra-high-speed imaging (delay between each image is 3.3 µs) for Monobond Etch & Prime sample until failure (failure load: 7,560 N). Focus on the failure mechanism: (A) first visible event: bleaching at resin bonding interface, (B) crack initiation highlighted by Edge Laplacian filtering, (C) slippage of the ceramic, (D) crack propagation and resin bonding bleaching, (E) following slippage, and (F) crack propagation highlighted by Edge Laplacian filtering.

The first event observed for MEP6 was a sudden bleaching that occurred in the resin bonding interface near the center of the sample (labeled t3.3 µs in Fig. 4). The previous frame was defined as the reference time (t0). Then, in the upper right corner, the resin bonding interface bleached and a first crack appeared in ceramic (t6.6 µs). At t9.9 µs, the identified bleached zone increased and a relative displacement (slippage) of the 2 ceramic parts and resin occurred in the lower left corner. For t13.2 µs, the displacement stepped up and the resin bonding interface bleached in the same area. The following images rom 16,5 µs to 46,2 µs (in Fig. 4) show the catastrophic failure resulting from the initial rupture.

The time code was defined similarly for all samples. For the MB6 sample (Figure 5), the first event observed occurred in the lower left corner. A slight slippage was visualized (labeled t3.3 µs in Fig. 5), becoming larger at t6.6 µs, when a ceramic crack appeared near the center of the sample. From t9.9 µs to t13.2 µs, resin bonding interface bleached in the upper right corner and slippage still extended. The following images from 16,5 µs to 46,2 µs show the catastrophic failure resulting from the initial rupture.

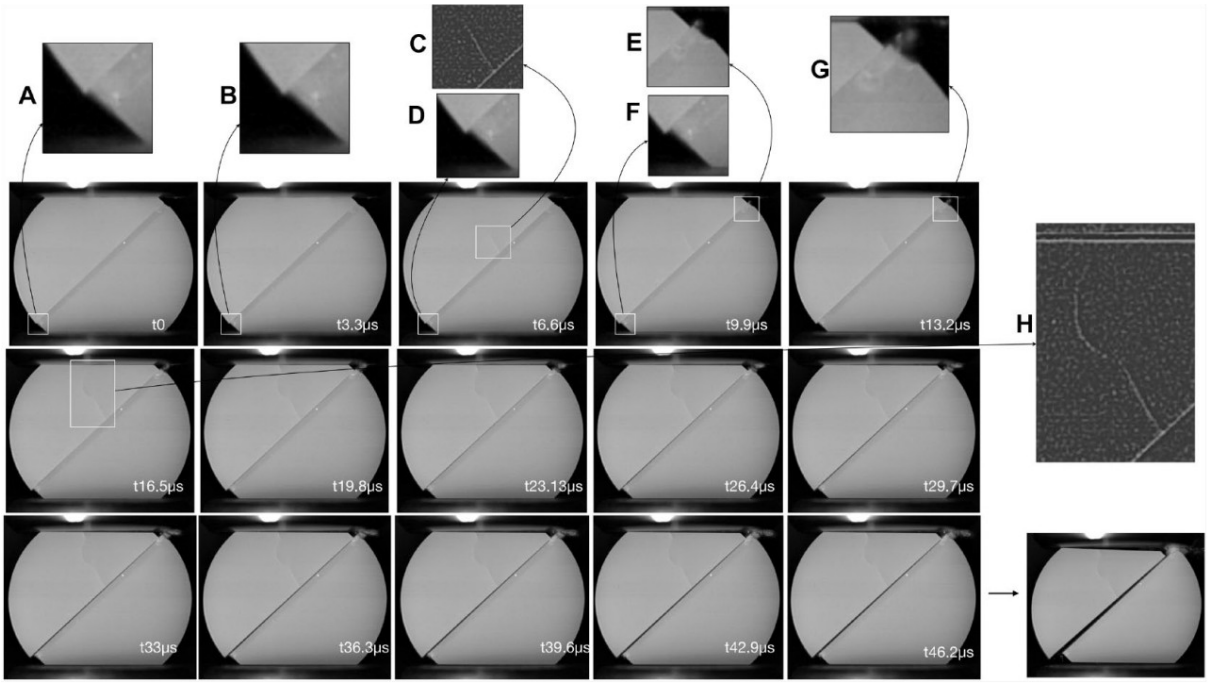

Figure 5. Sequence of successive images recorded by ultra-high-speed imaging (delay between each image is 3.3 µs) for Monobond Plus sample until failure (failure load: 7,435 N). Focus on the failure mechanism: (A) initial situation, (B) first visible event: slippage of the ceramic, (C) crack initiation highlighted by Edge Laplacian filtering, (D) following slippage, (E) bleaching at resin bonding interface, (F) following slippage, (G) following displacement and bleaching at resin bonding interface, and (H) crack propagation highlighted by Edge Laplacian filtering.

4 Discussion

The observation in Figure 3 reveals that the sample preparation protocol has a negligible impact on the overall shape of the force-displacement curves. The stiffness in each sample (Fig. 3), for both MB and MEP, is around 16 kN/mm with a low standard deviation. Such a result was expected as the bonding procedure has no influence on the macro-homogeneous response of the material. Despite the mechanical test being able to assess the impact of the bonding protocol on the shear–compression strength, results evidenced no significant differences between MB and MEP samples for both strength and stiffness as expressed by the high P values (0.34; respectively, 0.49) calculated with a 2-tailed Student's test (the level of significant difference being set at 0.05). The meticulous analysis of UHSI images by high digital zoom and slow motion scrutiny makes it possible to characterize and decompose the failure mechanism. As shown in Figures 4 and 5, it is already possible to observe that the first occurring event is a modification inside the resin bonding interface followed by catastrophic failure.
Then, the succession of images shows that, even if secondary cracks can occur in the ceramic or in the bonded layer, the principal crack, leading to the catastrophic failure of the whole sample, propagates at the interface between ceramic and the bonded layer (see Figures 4 and 5 and multimedia components). Thanks to the extreme

frame rate, the speed failure was calculated. The slippage speed was about 10 m/s while the crack propagation can reach about 150 m/s for the crack, appearing up to 1,000 m/s when the crack develops. The FEA put forward the combined shear and compressive stress at the interface (Fig. 2). The shear stress led to the slippage of the materials at rupture while the compressive stress prevented their separation, resulting in a micro-displacement of the upper half-disk downward (Figs. 4 and 5). Secondary cracks appeared subsequently by strength transfer initiated by debonding in the resin bonding interface. For all tested samples, cracks started at the interface toward press jaws.

Such events have never been clearly and entirely recorded and described. UHSI studies on dental material behavior are unusual. Griffith et al. (2000) first used UHSI coupled to a mechanical test. Composite restoration bonded on dentin was submitted to SBS without drawing any conclusion on the bonding interface failure mechanism. Forquin and Ando (2017) used UHSI to analyze the quantification of fragmentation in ceramics after impact loading. Hosaka et al. (2019) observed with USHI the bonding interface of dentin and restorative composite in μTBS. They concluded, “UHS videography with even higher frame rate and resolution can help in understanding the mechanism of fracture dynamics.”

In this study, the used camera had a much higher frame rate and resolution than those used by Hosaka. Moreover, a shear compression test was operated to get closer to physiologic and pathologic (bruxism) stresses. With this objective, shear and compression cannot be dissociated due to the mastication functionality to reduce the alimentary bolus.

Results for MB and MEP (Fig. 3 and Appendix Table) suggest that the MEP treatment slightly improves the bonding strength of the specimens while reducing dispersion of the results. Clinicians seek materials with the easiest protocol leading to repeatable results in order to ensure a serene daily activity. In this study, the intaglio pretreatment did not seem to have any significant impact on the macro-homogeneous mechanical response; the mean shear–compression strength was 7,850 N (SD = 1,420 N) for MB and 8,690 N (SD = 860 N) for MEP (Fig. 3 and Appendix Table). These results seem consistent with the literature (Román-Rodríguez et al. 2017; Wille et al. 2017; Dönmez et al. 2018; Lyann et al. 2018; Prado et al. 2018; Lopes et al. 2019; Vichi et al. 2021). Using SBS tests, Román-Rodríguez et al. (2017) obtained higher data for MB with greater homogeneity than MEP without a statistically significant difference. Alrahlah et al. (2017), also with SBS tests, combined with universal adhesive, obtained higher values for MEP than MB without a statistically significant difference. Slight differences between MEP and MB bond strength tests are reported in the literature but without statistically significant differences. Vichi et al. (2021) obtained similar results for μSBS with LiSi2 conditioned by HF and HF + Silane and questioned the usefulness of applying silane after HF etching in clinical situations. Furthermore, for these authors, MEP and MB performed comparable bond strength values, and the choice should “be based on other factors.”

5 Conclusion

Thanks to UHSI technological evolutions, this study shows that failure of bonded LiSi2 submitted to compression–shear strength is first due to debonding followed by catastrophic failure. Higher frame rate associated with sufficient camera resolution allowed us to visualize for the first time the failure mechanism. This

work highlights the usefulness of UHSI in dental research and begins to provide concrete answers to a major clinical prosthodontic problem. FEA indicated the interest of our original 45° resin bonding LiSi2 sample. The resulting shear–compression stress induced to the resin bonding interface draws closer from the clinical situation than other mechanical tests. Moreover, within the limits of this study, the nontoxic alternative pretreatment (MEP) shows a similar mechanical behavior to the gold standard (MB). Catastrophic failure results with no significant difference indicate MEP as an alternative to the gold standard in clinical practice. Thus, UHSI appears as a first-rate investigation protocol for a study of dental material mechanical behavior. It paves the way to new research possibilities in dental mechanics and biomechanics. New investigations are in progress with dental sample–bonded CARs.

Author Contributions

H. Lambert, S. Corn, R. Léger, P. Slangen, M. Fages, contributed to conception and design, data acquisition, analysis, and interpretation, drafted and critically revised the manuscript; P. Ienny, contributed to conception and design, data analysis, and interpretation, critically revised the manuscript. All authors gave their final approval and agree to be accountable for all aspects of the work.

Acknowledgments

The ceramic, conditioning, and bonding materials were generously supplied by the manufacturer (Ivoclar Vivadent AG). The authors thank Ametek Phantom France for lending the Phantom TMX7510 high-speed camera during the test period. They express their thanks and appreciation to Guillaume Ounoughi for his help with laboratory procedures.

Declaration of Conflicting Interests

The authors declared no potential conflicts of interest with respect to the research, authorship, and/or publication of this article.

Funding

The authors received no financial support for the research, authorship, and/or publication of this article.

ORCID iD

H. Lambert https://orcid.org/0000-0002-4160-9491

References

Alrahlah A, Awad MM, Vohra F, Al-Mudahi A, Al jeaidi ZA, Elsharawy M. 2017. Effect of self etching ceramic rimer and universal adhesive on bond strength of lithium disilicate ceramic. J Adhes Sci Technol. 31(23):2611–2619.

Blatz MB, Sadan A, Kern M. 2003. Resin-ceramic bonding: a review of the literature. J Prosthet Dent. 89(3):268–274.

Breschi L, Mazzoni A, Ruggeri A, Cadenaro M, Di Lenarda R, De Stefano Dorigo E. 2008. Dental adhesion review: aging and stability of the bonded interface. Dent Mater. 24(1):90–101.

Burke FJT. 1999. Fracture resistance of teeth restored with dentin-bonded crowns constructed in a leucite-reinforced ceramic. Dent Mater. 15(5):359–362.

Chi A, Wong H, Tian T, Kit J, Tsoi H, Francis M, Pekka J. 2017. Aspects of adhesion tests on resin–glass ceramic bonding. Dent Mater. 33(9):1045–1055.

Dapieve KS, Machry RV, Pilecco RO, Kleverlaan CJ, Rocha Pereira GK, Venturini AB, Valandro LF. 2020. One-step ceramic primer as surface conditioner: effect on the load-bearing capacity under fatigue of bonded lithium disilicate ceramic simplified restorations. J Mech Behav Biomed Mater. 104:103686.

Decerle N, Bessadet M, Munoz-Sanchez ML, Eschevins C, Veyrune J, Nicolas E. 2014. Evaluation of Cerec endocrowns: a preliminary cohort study. Eur J Prosthodont Restor Dent. 22(2):89–95.

Dejak B, Mlotkowski A. 2008. Three-dimensional finite element analysis of strength and adhesion of composite resin versus ceramic inlays in molars. J Prosthet Dent. 99(2):131–140.

Dönmez MB, Yucel MT, Kilic I, Okutan Y. 2018. Novel ceramic primer vs. conventional treatment methods: effects on roughness and bond strength of all-ceramic restorations. Am J Dent. 5(31):249–252.

El-Damanhoury HM, Gaintantzopoulou MD. 2018. Self-etching ceramic primer versus hydrofluoric acid etching: etching efficacy and bonding performance. J Prosthodont Res. 62(1):75–83.

Fages M, Bennasar B. 2013. The endocrown: a different type of all-ceramic reconstruction for molars. J Can Dent Assoc. 79:d140.

Fages M, Corn S, Slangen P, Raynal J, Ienny P, Turzo K, Cuisinier F, Durand JC. 2017. Glass ceramic CAD/CAM crowns and severely altered posterior teeth: a three levels study. J Mater Sci Mater Med. 28(10):145.

Fages M, Raynal J, Tramini P, Cuisinier F, Durand J-C. 2017. Chairside computer-aided design/computer-aided manufacture all-ceramic crown and endocrown restorations: a 7-year survival rate study. Int J Prosthodont. 30(6):556–560.

Forquin P, Ando E. 2017. Application of microtomography and image analysis to the quantification of fragmentation in ceramics after impact loading. Philos Trans A Math Phys Eng Sci. 375(2085):20160166.

Griffiths BM, Watson TF, Pagliari DE, Pilecki P, Sherriff M. 2000. Video rate confocal microscopic imaging of dentin/adhesive interfacial failure under load. Am J Dent. 13(5):271–279.

Guggenbühl S, Alshihri A, Husain NAH, Özcan M. 2021. Adhesion of resin-resin and resin–lithium disilicate ceramic: a methodological assessment. Materials (Basel). 14(14):3870.

Guimarães HAB, Cardoso PC, Decurcio RA, Monteiro LJE, De Almeida LN, Martins WF, Magalhães APR. 2018. Simplified surface treatments for ceramic cementation: use of universal adhesive and self-etching ceramic primer. Int J Biomater. 2018:2598073.

Hosaka K, Tichy A, Ikeda M, Nakagawa K, Sadr A, Tagami J, Takahashi M, Sato K, Nishitani Y, Klein-Junior CA, et al. 2019. Ultra-high-speed videography of resin–dentin interface failure dynamics under tensile load. Dent Mater. 35(7):153–161.

Kalavacharla V, Lawson N, Ramp L, Burgess J. 2015. Influence of etching protocol and silane treatment with a universal adhesive on lithium disilicate bond strength. Oper Dent. 40(4):372–378.

Lafuente D. 2012. SEM analysis of hybrid layer and bonding interface after chlorhexidine use. Oper Dent. 37(2):172–180.

Lise D, Perdigão J, Van Ende A, Zidan O, Lopes GC. 2015. Microshear bond strength of resin cements to lithium disilicate substrates as a function of surface preparation. Oper Dent. 40(5):524–532.

Lopes GC, Perdigão J, Baptista D, Ballarin A. 2019. Does a self-etching ceramic primer improve bonding to lithium disilicate ceramics? Bond strengths and FeSEM analyses. Oper Dent. 44(2):210–218.

Lyann SK, Takagaki T, Nikaido T, Uo M, Ikeda M, Sadr A. 2018. Effect of different surface treatments on the tensile bond strength to lithium disilicate glass ceramics. J Adhes Dent. 20(3):261–268.

Magne P, Douglas W. 1999. Porcelain veneers: dentin bonding optimization and biomimetic recovery of the crown. Int J Prosthodont. 12(2):111–121.

Magne P, Magne M, Belser U. 1999. The esthetic width in fixed prosthodontics. J Prosthodont. 8(2):106–118.

Maier E, Bordihn V, Belli R, Taschner M, Petschelt A, Lohbauer U, Zorzin J. 2019. New approaches in bonding to glass-ceramic: self-etch glass-ceramic primer and universal adhesives. J Adhes Dent. 21(3):209–217.

Özcan M, Allahbeickaraghi A, Dündar M. 2012. Possible hazardous effects of hydrofluoric acid and recommendations for treatment approach: a review. Clin Oral Investig. 16(1):15–23.

Pineda-Vásquez L, Fons-Font A, Bustos-Salvador JL, Alonso-Pérez-Barquero J, Román-Rodríguez JL. 2019. Shear bond strength of debonded ceramic restorations re-cemented by means of a cleaning and retreatment protocol. J Clin Exp Dent. 11(6):e506–e511.

Prado M, Prochnow C, Marchionatti AME, Baldissara P, Valandro LF, Wandscher VF. 2018. Ceramic surface treatment with a single-component primer: resin adhesion to glass ceramics. J Adhes Dent. 20(2):99–105.

Román-Rodríguez JL, Perez-Barquero JA, Gonzalez-Angulo E, Fons-Font A, Bustos-Salvador JL. 2017. Bonding to silicate ceramics: conventional technique compared with a simplified technique. J Clin Exp Dent. 9(3):e384–e386.

Sidhu SK, Sherriff M, Watson TF, Griffiths BM, Watson TF, Pagliari DE, Pilecki P, Sherriff M. 1999. Failure of resin-modified glass-ionomers subjected to shear loading. J Dent. 27(5):373–381.

Siqueira FSF, Campos VS, Wendlinger M, Muso RAC, Gomes JC, Reis A, Cardenas AFM, Loguercio AD. 2019. Effect of self-etching primer associated to hydrofluoric acid or silane on bonding to lithium disilicate. Braz Dent J. 30(2):171–178.

Venturini AB, Prochnow C, Pereira GKR, Segala RD, Kleverlaan CJ, Valandro LF. 2019. Fatigue performance of adhesively cemented glass-, hybrid- and resin-ceramic materials for CAD/CAM monolithic restorations. Dent Mater. 35(4):534–542.

Vichi A, Fabian Fonzar R, Carrabba M, Louca C, Scotti N, Mazzitelli C, Breschi L, Goracci C. 2021. Comparison between hydrofluoric acid and single-component primer as conditioners on resin cement adhesion to lithium silicate and lithium disilicate glass ceramics. Materials (Basel). 14(22):6776.

Wille S, Lehmann F, Kern M. 2017. Durability of resin bonding to lithium disilicate and zirconia ceramic using a self-etching primer. J Adhes Dent. 19(6):491–496.

Yao C, Ahmed MH, Yoshihara K, Mercelis B, Parise Gré C, Van Landuyt KL, Huang C, Van Meerbeek B. 2019. Bonding to enamel using alternative enamel conditioner/etchants. Dent Mater. 35(10):1415–1429.

Yu Y, Wang R. 2008. Observation on bonding interface of sclerotic dentin with confocal laser scanning microscope. West China J Stomatol. 26(3): 258–261.